Nanotribology and Nanoscale Friction

Smooth sliding and modification of frictional characteristics through feedback control

Yi Guo, Zhihua Qu, Yehuda Braiman, Zhenyu Zhang, and Jacob Barhen

Tribology is the science and technology of interacting solid surfaces in relative motion, and its topics include the study of lubricants, lubrication, friction, wear, and bearings. It is estimated that friction and wear cost the US economy 6% of the gross national product [1]. For example, 5% of the total energy generated in an automobile engine is lost to frictional resistance. Also notable are many tribology issues in the human body. The study of nanoscale friction has technological impacts in reducing energy loss in machines, in microelectromechanical systems (MEMS), and in the development of durable and low-friction surfaces and ultra thin lubrication films.

Friction between contacting surfaces is a longstanding and crucially important scientific problem, which is characterized by interplays between energy, stress, and chemistry at many length scales. To understand friction and to meet technology needs, knowledge from the fields of chemistry, material science, physics, mathematics, and engineering must be applied. Fundamental scientific questions include how energy is dissipated in nonequilibrium processes and how the course of energy dissipation can be intentionally controlled. The roadmap between friction,

which is an ensemble-averaged quantity, and molecule-level dynamics remains open. These issues enable the development of many energy-efficient technologies, such as ultra-thin lubricant films for ultra-high-temperature lubrication and for control and manipulation of frictional properties during sliding.

Friction is intimately related to both adhesion and wear, which are nonequilibrium and multiscale phenomena, from the atomic level to the molecular level and to the microscopic level. As such, multidisciplinary studies are required to reveal the nature of sliding on a variety of surfaces (smooth or rough, elastic, viscoelastic or plastic, dry or lubricated) that possess different chemistry. Some of the outstanding issues and questions are [2]:

- Experimental and theoretical elucidation of linear characteristics of friction at or near an equilibrium point, and their relation to modern statistical-mechanical theories of solids and liquids at the equilibrium.
- Elucidation of nonlinear characteristics of friction away from the equilibrium and the extension to modern experimental frontiers of definitive analysis, to modern theories of complexity, and to modern computational resources.
- Can we develop theory that is beyond empiricism and able to predict what makes lubricant molecules of one chemical structure more effective in lowering friction forces than others?
- How can we design tribological surfaces with desired frictional properties, that is, principles for surface engineering? How can we control frictional properties while sliding so as to gain desired friction characteristics?
- Friction and lubrication at extreme conditions such as high-temperature or nonequilibrium or nanoconfinement, phenomena still to be understood such as stick-slip boundary conditions

at the macroscale, tribo-charging, triboluminescence, and quantum effects in tribology, and performances of whole tribosystems based on their constituent parts.

In light of their challenges in the area of tribology, we focus in this article on modeling and control of friction, so that the closed-loop frictional dynamics produce a given desirable motion. In the following, we describe the model systems, formulate the control problem, present two control strategies, and conduct detailed analysis of single-particle dynamics in the open-loop and closed-loop systems. Experimental setup and recent experimental results are also shown.

FRICTION CONTROL AT THE NANOSCALE

Friction can be controlled by applying small perturbations to accessible elements and parameters of the sliding system [3], [4], [5], [6], [7], [8]. Implementation of the corresponding control requires *a priori* knowledge of the strength and timing of the perturbations, but general techniques have not been developed yet. Moreover, experimental limitation in designing friction control may be severe. Recently, it is shown in [5] and [6] that friction in thin-film boundary-lubricated junctions can be reduced by coupling small-amplitude directional periodical mechanical oscillations of the confining boundaries to the molecular degree of freedom of the sheared interfacial lubricating fluid. Using a surface-force apparatus modified to measure friction forces while simultaneously inducing normal vibrations between two boundary-lubricated sliding surfaces, load- and frequency-dependent transitions between dynamical friction states are observed in [6]. In particular, these observations reveal regimes of vanishingly small friction at interfacial oscillations.

Effects of periodic and random surface oscillations on frictional properties of surfaces are studied using an atomic force microscope (AFM) [9]. Since the first measurement of friction reported in [10], AFM has been widely used to measure frictional properties of materials at the nanometer scale [11], [12]. As in the surface-force apparatus experiments, a significant reduction in the friction force and vanishingly small friction as a result of surface oscillations are observed [9], [13]. Methods are considered in [7] to control friction in a system under shear so that chaotic stick-slip motion is eliminated. Significant changes in frictional responses are observed in the two-plate model [14] by modulating the normal response to lateral motion [8]. In addition, surface roughness and thermal noise are expected to play a significant role in deciding control strategies at the micro and the nano scales [15], [16].

In this article, two types of controllers, namely, the non-Lipschitzian method of control and the Lyapunov-based control, are investigated for friction control. The frictional dynamics are assumed to be described by the Frenkel-Kontorova (FK) model, which is the subject of the next section.

THE SYSTEM MODEL

Frenkel-Kontorova model describes dynamics of a chain of particles whose interactions are between the nearest neighbors and which are subjected to an external periodic potential. The model can be used as a general framework to describe friction [1], and its complexity varies from simplified 1D model to 2D and 3D models, and to a full set of molecular equations. In addition, the FK model is applied in [17] to additional physical systems, including charge-density waves, magnetic spirals, and absorbed monolayers.

As reviewed in [17], the FK model can be traced back to the simple model studied by Prandtl and Dehlinger in 1928 and 1929. The FK model was independently introduced by Frenkel and Kontorova in 1938. The FK model is used in this article, which can be derived for the corresponding chain of particles depicted schematically in Figure 1. The equation of motion for this 1D array of N identical particles moving on a surface can be derived as

$$m\ddot{x}_i + \gamma\dot{x}_i = -\frac{\partial U(x_i)}{\partial x_i} - \frac{\partial W(x_i - x_j)}{\partial x_i} + f + \eta(t), \quad i = 1, \ldots, N, \tag{1}$$

where x_i is the position coordinate of the ith particle, m is the mass of the particle, $\gamma > 0$ is the friction coefficient characterizing the energy exchange between the single particle and the substrate, f is the external force applied, $\eta(t)$ is the thermal noise, $U(x_i)$ is the periodic potential applied by the substrate, and $W(x_i - x_j)$ is the inter-particle interaction potential.

Under the simplifications that the substrate potential has the form of $\frac{1}{2\pi}(1 - \cos 2\pi x_i)$, that the same force is applied to each particle, and that there is no noise (in order to focus on the deterministic behavior), (1) reduces to the simplified FK model [3], [18]

$$\ddot{z}_i + \gamma\dot{z}_i + \sin(z_i) = f + F_i, \tag{2}$$

where $z_i = 2\pi x_i$ is the dimensionless phase variable and F_i is the nearest-neighbor interaction force. A common choice of F_i is the Morse-type interaction

$$F_i = \frac{\kappa}{\beta}\left\{e^{-\beta(z_{i+1}-z_i)} - e^{-2\beta(z_{i+1}-z_i)}\right\} - \frac{\kappa}{\beta}\left\{e^{-\beta(z_i-z_{i-1})} - e^{-2\beta(z_i-z_{i-1})}\right\}, \tag{3}$$

where $i = 2, \ldots, N-1$, κ and β are positive constants, while the free-end boundary conditions are

$$\begin{aligned} F_1 &= \frac{\kappa}{\beta}\left\{e^{-\beta(z_2-z_1)} - e^{-2\beta(z_2-z_1)}\right\}, \\ F_N &= -\frac{\kappa}{\beta}\left\{e^{-\beta(z_N-z_{N-1})} - e^{-2\beta(z_N-z_{N-1})}\right\}. \end{aligned} \tag{4}$$

In the limit $\beta \to 0$, the forces in (3) and (4) become

$$F_i \;=\; \kappa\left(z_{i+1} - 2z_i + z_{i-1}\right), \tag{5}$$

where $i = 2, \ldots, N-1$, and

$$F_1 = \kappa(z_2 - z_1), \qquad F_N = \kappa(z_{N-1} - z_N). \tag{6}$$

Various experimental techniques are used today to gain fundamental insights into friction. These techniques include surface-force apparatus (SFA), quartz-crystal microbalance (QCM), and AFM. An AFM experimental setup is described in the section "Physical Experiments". The AFM experimental model imitates the AFM tip as a 1D array of particles moving on a rigid substrate. As a natural extension of single particle model of the AFM tip [19], [20], the model is given as [9]

$$\ddot{z}_i + \gamma\dot{z}_i + \sin(z_i) \;=\; \alpha(v_0 t - z_{cm}) + F_i, \tag{7}$$

where α is a positive constant depending on the AFM cantilever, v_0 is the constant driving velocity of the AFM tip, z_{cm} is the position variable of the center of mass, and F_i is the Morse interaction force in the form of (3) and (4).

In what follows, model (2) is used to describe the QCM experiments, and model (7) is applied to describe AFM and SFA experiments. In the QCM model, the applied force acts as an external variable that can be controlled experimentally, while the velocity of the center of mass is the function of the external force. On the contrary, in SFA and AFM experiments, the driving velocity is the externally control variable and the friction force is a function of the driving velocity. The two models are closely related. More details on the AFM experimental implementation is discussed in the section "Physical Experiments".

CONTROL PROBLEM FORMULATION

Control at the nanoscale presents many challenges. For example, due to strict confinement and additional constraints, nanosystems are not readily accessible, and not all particles can be targeted or controlled individually. It would be sufficient that the nanosystem be controlled as a whole. Also, their characteristic times may be very short, sometimes significantly shorter than those of the available control devices. These phenomena occur in the control of friction at the nanoscale. Nonetheless, feedback control can be considered [18].

To consider the control problem, a control variable $u(t)$ in terms of external force is added into the QCM system model (2) [18]

$$\ddot{z}_i + \gamma \dot{z}_i + \sin(z_i) \quad = \quad f + F_i + u(t). \tag{8}$$

In QCM experiments, only the position z_{cm} and velocity v_{cm} are measured. These variables are given by

$$v_{cm} = \frac{1}{N}\sum_{i=1}^{N} \dot{z}_i, \quad z_{cm} = \frac{1}{N}\sum_{i=1}^{N} z_i.$$

Thus, the feedback control $u(t)$ can only be a function of these two measurable quantities, and the control problem based on the QCM model (2) becomes to design a feedback control law

$$u(t) \quad = \quad u(v_{target}, v_{cm}, z_{cm}), \tag{9}$$

such that v_{cm} tends to v_{target}, where v_{target} is a constant commanded velocity.

Similarly, adding control $u(t)$ into the AFM model (7) yields

$$\ddot{z}_i + \gamma \dot{z}_i + \sin(z_i) \quad = \quad \alpha(v_0 t - z_{cm}) + F((z_{i+1} - z_i), (z_i - z_{i-1})) + u(t). \tag{10}$$

The measurable quantity in the above AFM experiments is $\alpha(z_{cm} - v_0 t)$, which is proportional to the friction force. Assuming that the derivative of $\alpha(z_{cm} - v_0 t)$ is available real time, the control problem is to find the feedback control law $u(z_{cm}, \dot{z}_{cm}, t)$ such that $\alpha(z_{cm} - v_0 t)$ is made as small as possible.

In what follows, two control problems are presented, and the results based on the two models are closely matched. In the next section, we begin with control design for the QCM model while its extension to the AFM model is presented in the subsequent section.

FEEDBACK CONTROL DESIGN FOR THE QCM MODEL

Several control strategies are studied in literature for the control problem formulated above. Here, we describe and compare two representative feedback control schemes.

Non-Lipschitzian Control

A feedback control algorithm is considered in [18], and it is based on the concept of terminal attractor, which is usually associated with non-Lipschitzian dynamics. The non-Lipschitzian control is given by

$$u(t) \;=\; \alpha(v_{target} - v_{cm})^{\xi}, \tag{11}$$

where α is a positive constant, $\xi = 1/(2n+1)$ and n is a positive integer.

Control law (11) is capable of making the velocity of the center of mass converge to the targeted value, its value remains to be small, and the resulting transient time is short. These properties can be illustrated using the concept of terminal attractor. For instance, if $\xi = 1/7$, the

control has an equivalent gain of

$$\frac{du(t)}{dv_{cm}} = -\frac{1}{7}\alpha(v_{target} - v_{cm})^{-\frac{6}{7}}, \tag{12}$$

which goes to $-\infty$ as v_{cm} tends to v_{target}. The "infinite attraction power" of the non-Lipschitzian attractor makes it possible to achieve fast response. Interested readers are referred to [21], [22] for in-depth discussions on non-Lipschitzian dynamics and their finite time convergence.

In order to achieve the desired attractor, control (11) is modified in [18] as

$$\begin{aligned} u(t) &= \alpha(v_{target} - v_{cm})^{\xi} - \rho(v_{av} - v_{cm})^{\xi} \times sgn\left((v_{av} - v_{cm})(v_{cm} - v_{target})\right) \\ &\quad \times H[r - \|v_{target} - v_{av}\|], \end{aligned} \tag{13}$$

where v_{av} is the average velocity that represents the moving runtime average of v_{cm}, $H(\cdot)$ denotes the Heaviside function defined by $H(z) = 1$ for $z > 0$ and $H(z) = 0$ for $z < 0$. The second term in (13) is a repelling force that drives the trajectory towards the target velocity and away from possible natural attractors of system dynamics. This effect of the controller is illustrated by the simulation results shown in the next section.

Control (13) provides the first and an intuitive feedback scheme to stabilize the average tracking system. This controller has the advantages of fast responding time, small control effort, and robustness. On the other hand, its disadvantages are that it can only attract the velocity to a vicinity of the commanded value and that persistent fluctuations may be present, which is shown in the simulation results of the next section.

Control Design using Lyapunov Stability Methods

Motivated by [18], a smooth control is designed in [23] using Lyapunov direct method. Define tracking error variables

$$e_{i1} = z_i - v_{target}t, \qquad e_{i2} = \dot{z}_i - v_{target}, \tag{14}$$

and average tracking error variables

$$e_{1av} = z_{cm} - v_{target}t, \qquad e_{2av} = v_{cm} - v_{target}. \tag{15}$$

Then, dynamics of the average tracking error system can be written as

$$\begin{aligned} \dot{e}_{1av} &= e_{2av} \\ \dot{e}_{2av} &= -\frac{1}{N}\sum_{i=1}^{N}\sin(e_{i1} + v_{target}t) - \gamma(e_{2av} + v_{target}) + u(t). \end{aligned} \tag{16}$$

Inter-particle interaction terms $F_i(\cdot)$ are canceled in the above average system.

It is shown in [23] that the smooth feedback control for the average error system is

$$u(t) = -f + \gamma v_{target} - k_1(z_{cm} - v_{target}t) - k_2\left(v_{cm} - v_{target}\right) + \sin(v_{target}t), \tag{17}$$

where k_1, k_2 are positive constants. (17) is synthesized through stability analysis of the closed-loop system using Lyapunov theory. That is, considering the quadratic Lyapunov function candidate

$$V(t, e_{av}) = \frac{1}{2}e_{1av}^2 + \frac{1}{2}(c_1 e_{1av} + e_{2av})^2, \tag{18}$$

where $c_1 > 0$, it follows that, under control (17), its time derivative along the trajectory of closed-loop average dynamics is

$$\dot{V} \leq -c_1\left[e_{1av}^2 + c_1(e_{1av} + e_{2av})^2\right] + \frac{1}{c_2}, \tag{19}$$

which is negative definite for large values of tracking errors. Inequality (19) guarantees that the average error-state variables, e_{1av} and e_{2av}, are uniformly bounded ([24], [25]). Further analysis of inequality (19) renders the ultimate bound on e_{1av} and e_{2av} [26]

$$b \;=\; \sqrt{\frac{1}{c_1 c_2 \lambda_{min}(P)}}, \tag{20}$$

where $\lambda_{min}(P)$ is the minimum eigenvalue of P, and P is a positive-definite matrix defined by

$$P = \begin{bmatrix} 1 + c_1^2 & c_1 \\ c_1 & 1 \end{bmatrix}.$$

Thus, c_1, c_2 can be adjusted through the selection of k_1 and k_2 to meet certain desired performance. In (19) and (20), parameters c_1 and c_2 are related to control parameters k_1 and k_2 as

$$k_1 = c_1^2 + c_1 c_2 + 1, \qquad k_2 = 2c_1 + c_2 - \gamma. \tag{21}$$

We can see that there is a tradeoff between the size of the ultimate bound and the control effort, big control effort gives a small bound, and tracking errors of the average system become smaller than the ultimate bound in a finite time.

To make the error state (e_{1av}, e_{2av}) converge to zero, control law (17) can be modified as

$$u(t) \;=\; \gamma v_{target} - k_1(z_{cm} - v_{target}t) - k_2\left(v_{cm} - v_{target}\right) + \sin(v_{target}t) - 2sgn(\xi), \tag{22}$$

where $sgn(\xi)$ is the signum function defined as $sgn(\xi) = 1$ for $\xi > 0$, $sgn(\xi) = -1$ for $\xi < 0$, and $sgn(\xi) = 0$ for $\xi = 0$. With the last and switching term in (22), the time derivative of the Lyapunov function is negative definite, which ensures asymptotic stability of the closed-loop system. However, control (22) is again non-Lipschitzian.

The Lyapunov argument outlined above provides a systematic design method for synthesizing stabilizing control laws. Control laws (17) and (22) guarantee uniform boundedness and asymptotic stability of the error state, respectively. The control parameters are directly related to the system performance, and precise control can be achieved. It is worth noting that a switching control may cause chatting along its switching surface [27].

FEEDBACK CONTROL DESIGN FOR THE AFM MODEL

QCM model (8) and AFM model (10) are closely related. For AFM model (10), control can be chosen to be

$$u(t) \;\; = \;\; \gamma v - k\left(\dot{z}_{cm} - v_0\right) + \sin(v_0 t), \tag{23}$$

where k is a positive constant. Control (23) guarantees that the friction force is bounded, and, more specifically, smaller than a positive constant which depends on parameters α and k. To verify the result, note that control (23) together with the first term of the right side of (7) is actually feedback control (17). Thus, the ultimate bound for the error signal $\|(z_{cm} - v_0 t)^2 + [c(z_{cm} - v_0 t) + (\dot{z}_{cm} - v_0)]^2\|$ is again that in (20).

If the switching term $-2sgn[c(z_{cm}-v_0 t)+(\dot{z}_{cm}-v_0)]$ is introduced in (23), the measurable friction force $\alpha(z_{cm} - v_0 t)$ goes to zero, which is the ideal case of zero friction.

CHARACTERIZATION OF CONTROL PERFORMANCE

Numerical simulations are performed for the controllers described in the previous sections. Performance of non-Lipschitzian control (13) is shown in Figure 2, for convergence of velocity of

the center of the mass to several commanded values and for control histories. Clearly, persistent oscillation are present, while amplitude of control is relatively small.

Figure 3 shows performances of Lyapunov-based control (17). It can be seen that, with the price of higher control effort, oscillation is eliminated.

ANALYSIS OF SINGLE-PARTICLE DYNAMICS

In the above control designs, only average quantities, that is, the position and velocity of the center of mass, are considered. One may ask: how about individual particles? Are their closed-loop dynamics stable? To answer the questions, let us first investigate the open-loop stability properties of particles.

Local Stability of Open-Loop Systems

It follows from (2) that equilibrium points of individual particles without external force ($f = 0$) are at

$$z_i = l\pi, \quad \dot{z}_i = 0, \quad l = 0, \pm 1, \pm 2, \ldots \tag{24}$$

Since $f = 0$, equation (2) can be expressed in the state space as

$$\begin{aligned} \dot{x}_{i1} &= x_{i2} \\ \dot{x}_{i2} &= -\sin x_{i1} - \gamma x_{i2} + F_i, \end{aligned} \tag{25}$$

where $i = 1, 2 \ldots, N$, $x_{i1} = z_i, x_{i2} = \dot{z}_i$, and F_i is the Morse-type particle interaction.

Linearizing system (25) around its equilibrium points $(x_{i1}, x_{i2}) = (l\pi, 0)$ and stacking all

the state space equations yield the state-space representation in terms of Kronecker product [28]

$$\dot{x} \;=\; Ax + BFx, \tag{26}$$

where $x = [x_{11} - l\pi \; x_{12} \; x_{21} - l\pi \; x_{22} \; \ldots \; x_{N1} - l\pi \; x_{N2}]^T$,

$$A = I_N \otimes A_i, \quad B = I_N \otimes B_i, \quad F = Q \otimes \begin{bmatrix} \kappa & 0 \end{bmatrix}, \tag{27}$$

and

$$A_i = \begin{cases} \begin{bmatrix} 0 & 1 \\ -1 & -\gamma \end{bmatrix}, \text{when } l = 2k\pi, k = 0, \pm 1, \ldots, \\ \begin{bmatrix} 0 & 1 \\ 1 & -\gamma \end{bmatrix}, \text{when } l = (2k+1)\pi, \end{cases}$$

$$B_i = \begin{bmatrix} 0 \\ 1 \end{bmatrix}, \qquad Q = \begin{bmatrix} -1 & 1 & 0 & \ldots & 0 \\ 1 & -2 & 1 & 0 & \ldots \\ & & \vdots & & \\ 0 & \ldots & 1 & -2 & 1 \\ 0 & \ldots & 0 & 1 & -1 \end{bmatrix}. \tag{28}$$

It follows from

$$BF \;=\; (I_N \otimes B_i)(Q \otimes \begin{bmatrix} \kappa & 0 \end{bmatrix}) = (I_N Q) \otimes \left(B_i \begin{bmatrix} \kappa & 0 \end{bmatrix} \right) = Q \otimes \begin{bmatrix} 0 & 0 \\ \kappa & 0 \end{bmatrix}$$

that all the eigenvalues of BF are zero. In fact, linearized system (26) has a coupling between the neighbor particles. Connectivity of the particles can be described by a bidirectional graph as shown in Figure 4, whose Laplacian matrix [28] is $(-Q)$. Recall that the Laplacian matrix L_G is defined by $L_G = D - A$, where A is the adjacent matrix with diagonal entries 0 and

off-diagonal entries $a_{ij} = 1$ if there is a link from node i to node j, otherwise $a_{ij} = 0$; D is the degree matrix with diagonal entries $d_{ii} = \sum_{j=1}^{n} a_{ij}$ and off-diagonal entries 0.

It is not difficult to see that every isolated subsystem has stable equilibrium points at $(2k\pi, 0)$ and unstable equilibrium at $((2k+1)\pi, 0)$. In fact, without particle interaction, equation (25) becomes that of a pendulum equation in which case equilibrium points $(2k\pi, 0)$ correspond to stable downward positions and equilibrium points $((2k+1)\pi, 0)$ correspond to unstable upward positions [24]. The question naturally arising is what stability properties are in the presence of particle interactions.

To answer the above question, let us examine the structure properties of linear matrix $(A + BF)$ in (26). Since A is already block diagonal, a similarity transformation that maps BF into block diagonal, would allow us to conclude stability result in a straightforward manner. In light of connectivity graph and its Laplacian matrix $(-Q)$, such a transformation matrix can be easily found. Since Q is a real symmetric matrix, there exists a transformation matrix T such that $T^{-1}QT = D$, where D is a diagonal matrix of eigenvalues of Q. It can be shown that matrix $T \otimes I_2$ is the similarity transformation matrix for diagonalization of BF, that is,

$$(T \otimes I_2)^{-1}(BF)(T \otimes I_2) \;=\; D \otimes \begin{bmatrix} 0 & 0 \\ \kappa & 0 \end{bmatrix}, \tag{29}$$

where I_2 is the identity matrix of dimension 2.

Block diagonalization (29) can be used to determine stability. Recall that Q is a row-sum-zero matrix and whose off-diagonal elements are all negative. Hence, eigenvalues of matrix Q have the property [28], [29]

$$\mu_1 \leq \mu_2 \leq \ldots \leq \mu_{N-1} \leq \mu_N = 0. \tag{30}$$

Consequently, diagonal matrix D has nonpositive diagonal elements. It is easy to show that

$$(T \otimes I_2)^{-1}(A + BF)(T \otimes I_2) \quad = \quad H, \tag{31}$$

where H is a block diagonal matrix with the diagonal elements

$$H_{ii} \quad = \quad \begin{cases} \begin{bmatrix} 0 & 1 \\ -1 + \mu_i \kappa & -\gamma \end{bmatrix}, & \text{at equilibrium } (2k\pi, 0), \\ \begin{bmatrix} 0 & 1 \\ 1 + \mu_i \kappa & -\gamma \end{bmatrix}, & \text{at equilibrium } ((2k+1)\pi, 0). \end{cases} \tag{32}$$

In light of the inequality in (30), H has negative eigenvalues at the equilibrium points $(2k\pi, 0)$, and positive eigenvalues at others. Thus, we conclude that in the absence of external forces, the particle array is asymptotically stable at $(2k\pi, 0)$ and unstable at $((2k+1)\pi, 0)$ with and without particle interactions.

Stability of Single Particles in the Closed-Loop Tracking System

Upon revealing the result of open-loop stability, one may wonder if all the particles are stable under tracking control (17). The answer is not necessarily positive, and it can be easily seen from simulation results. Figure 5 shows individual-particle dynamics in a five-particle tracking control system. It can be seen that while the velocity of the center of mass asymptotically tracks the commanded velocity $v_{target} = 1.5$ and hence the average system is stable, individual particles are not stable.

To analytically determine individual-particle stability in the closed-loop tracking system, let us use the Lyapunov direct method again. Given the tracking error variables in (14), the

state-space model of the closed-loop system under control (17) is

$$\begin{aligned}
\dot{e}_{i1} &= e_{i2} \\
\dot{e}_{i2} &= -\gamma e_{i2} + F_i - \bar{k}_1 \left(\sum_{i=1}^{N} e_{i1} \right) - \bar{k}_2 \left(\sum_{i=1}^{N} e_{i2} \right) + \left[\sin(v_{target} t) - \sin(e_{i1} + v_{target} t) \right], \quad (33)
\end{aligned}$$

where $\bar{k}_1 = k_1/N$, and $\bar{k}_2 = k_2/N$.

System (33) is linear except for its sinusoidal terms, and these sinusoidal terms can be treated as nonlinear perturbations. Following the analysis of the open-loop system, it can be shown that the linear part of system (33) is locally asymptotically stable. Then, using robust control techniques [25], we can obtain stability conditions for the closed-loop system. Because the complete proof is lengthy, we choose to state the main result below and refer interested readers to [26] for details.

It is shown in [26] that closed-loop system (33) is asymptotically stable for large values of γ and κ. Specifically, if friction coefficient and particle-interaction parameter are chosen such that

$$\begin{aligned}
\kappa &> \frac{1}{\min_{i \leq N-1}(-\mu_i)}, \\
\gamma &> \frac{1}{\sqrt{\min_{i \leq N-1}(-\mu_i)\kappa - 1}}, \quad (34)
\end{aligned}$$

where $\mu_1, \ldots, \mu_{N-1}$ are negative eigenvalues of matrix Q, feedback control (17) ensures that all particles are stable around the commanded trajectory by simply choosing control gains as

$$\begin{cases}
k_1 \geq \kappa \min_{i \leq N-1}(-\mu_i), \\
k_2 \geq 0. \quad (35)
\end{cases}$$

The above result gives a sufficient condition on stabilizing individual particles along the commanded trajectories, and they match with the physics intuition that individual particles are

stabilized in their nominal sliding positions when particle interactions are strong enough such that Morse interactions are repulsive and the potential between the particles and the substrate is strong to lock the phase variables to their nominal positions. Since an application of Lyapunov direct method often yields sufficient stability conditions only, the stabilizing conditions provided above are sufficient and may be conservative.

To verify theoretical analysis, numerical simulations are carried out. Figure 6 shows individual particle trajectories in a three-particle tracking system.

PHYSICAL EXPERIMENTS

It is challenging to experimentally manipulate and control friction between sliding surfaces. Surface vibrations in both normal and lateral direction to manipulate friction has been employed in [5], [6], [7] and references therein. An experiment studying the effect of surface vibrations on frictional properties of surfaces and using an atomic force microscope is conducted at the Oak Ridge National Laboratory. That experimental setup and its main results are described below.

In the experiment, mercaptopropionic acid is used without any further purification. It is selected as a boundary lubricant because of its simple structure and hydrophilicity. An atomically smooth mica surface is cleaved, and a 2.5-nm thickness of chromium and a 30 nm thickness of gold layers are sequentially deposited on it. A self-assembled monolayer of mercaptopropionic acid is formed on a fresh gold surface by dipping the gold-coated mica into a 1 mg/ml concentration of ethanol solution overnight. After being thoroughly rinsed with ethanol and completely dried with clean nitrogen, the substrate is immediately mounted on a piezoelectric

actuator. The amplitude and frequency of vertical vibration by the actuator are controlled using a digital function generator.

To measure friction, an multimode AFM from Digital Instrument, Santa Barbara, CA equipped with a quadrant position-sensitive detector is used. A diode laser is focused on the end of the cantilever and aligned to reflect the laser beam to the center of the detector. Proportional and integral gains of a feedback loop are set to low values because high values can exert a large influence on the lateral force measurement. Scan speed and scan size are fixed at 1.97 Hz and 100 nm, respectively, during all the the measurements. Experimental results are shown in [9], [13] where a reduction of frictional force is observed using vertical vibration of the substrate.

The controllers developed in the article have not been tested experimentally yet. To implement the proposed control algorithms described in the section "Feedback Control Design for the AFM Model", we can use a piezoelectric actuator to provide external forces on the AFM tip or the substrate. A possible experimental setup is schematically illustrated in Figure 7. A very small tip attached on a cantilever is drawn across a surface. The surface is systematically scanned line by line. The tip is bent by the forces between the tip and the surface. This motion of the tip is detected with the same laser beam deflection method. The position of the beam is detected with a four-quadrant photodetector. The quadrant detector records the difference between the trace and retrace curves of the AFM tip, which is proportional to the frictional force. The friction force can be controlled by either driving velocity or surface vibration. This concept may not be a real-time setup, and additional research is required for real-time implementation of the control algorithms developed in this article.

CONCLUSIONS

In this article, friction control at the nanoscale has been studied using the Frenkel-Kontorova model. Two control design methods have been presented, namely, non-Lipschitzian control, and Lyapunov-based control. The control algorithms have been discussed in detail and could be directly applied to quartz-crystal microbalance experiments. For atomic force microscopy and surface-force apparatus experiments, a modification of the algorithms has been presented to reduce friction forces. In addition to analysis of average friction quantities, individual particle motions in both open-loop and closed-loop systems have been investigated. It is revealed that under certain and restrictive conditions on the system and control parameters, individual particles can also be stabilized. Experimental setup using AFM to measure friction has also been presented. Future research is needed on experimental implementation and testing of the developed control algorithms.

ACKNOWLEDGMENTS

Yi Guo is supported in part by the Center for Intelligent Networked Systems at Stevens Institute of Technology. The authors would like to acknowledge the support by the Nanotechnology Initiative at University of Central Florida (Yi Guo and Zhihua Qu), and the support by the U.S. Department of Energy, Grant No. DE-FG02-03ER46091 (Zhenyu Zhang), and the Division of Materials Sciences and Engineering (Yehuda Braiman, Zhenyu Zhang, Jacob Barhen), Office of Basic Energy Sciences, under contract DE-AC05-00OR22725 with Oak Ridge National Laboratory, managed and operated by UT-Battelle, LLC.

REFERENCES

[1] B. N. J. Persson. *Sliding Friction*. Springer, 2nd edition, 2000.

[2] Y. Braiman, P. Cummings, and S. Granick. Frontiers in tribology at the atomic and nano scales. White Paper, 2004.

[3] Y. Braiman, F. Family, and H. G. E. Hentschel. Nonlinear friction in the periodic stick-slip motion of coupled oscillators. *Physical Review B*, 55(5):5491–5504, 1997.

[4] A. Cochard, L. Bureau, and T. Baumberger. Stabilization of frictional sliding by normal load modulation: A bifurcation analysis. *Trans. ASME*, 70:220–226, 2003.

[5] J.P. Gao, W.D. Luedtke, and U. Landman. Friction control in thin-film lubrication. *J. Phys. Chem. B*, 102:5033–5037, 1998.

[6] M. Heuberger, C. Drummond, and J. N. Israelachvili. Coupling of normal and transverse motions during frictional sliding. *J. Phys. Chem. B*, 102:5038–5041, 1998.

[7] M. G. Rozman, M. Urbakh, and J. Klafter. Controlling chaotic friction. *Phy. Rev. E*, 57:7340–7443, 1998.

[8] V. Zaloj, M. Urbakh, and J. Klafter. Modifying friction by manipulating normal response to lateral motion. *Phyical Review Letters*, 82:4823–4826, 1999.

[9] S. Jeon, T. Thundat, and Y. Braiman. Fricitonal dynamics at the atomic scale in presence of small oscillations of the sliding surfaces. In A. Erdemir and J. M. Michel, editors, *Superlubricity*. Elsevier, in press.

[10] C. M. Mate, G. M. McClelland, R. Erlandsson, and S. Chiang. Atomic-scale friction of a tungsten tip on a graphite surface. *Physical Review Letters*, 59:1942–1945, 1987.

[11] S. Fujisawa, E. Kishi, Y. Sugawara, and S. Morita. Lateral force curve for atomic

force/lateral force microscope calibration. *Appli. Phys. Lett.*, 66:526–528, 1995.

[12] X. Yang and S. S. Perry. Friction and molecular order of alkanethiol self-assembled monolayers on Au(111) at elevated temperatures measured by atomic force microscopy. *Langmuir*, 19:6135–6139, 2003.

[13] S. Jeon, T. Thundat, and Y. Braiman. Effect of normal vibration on friction in the atomic force microscopy experiment. *Applied Physics Letters*, 88(1):214102.1–214102.3, 2006.

[14] M. G. Rozman, M. Urbakh, and J. Klafter. Stick-slip motion and force fluctuations in a driven two-wave potential. *Physical Review Letters*, 77:683–686, 1996.

[15] Y. Braiman, F. Family, H. G. E. Hentschel, C. Mak, and J. Krim. Tuning friction with noise and disorder. *Physical Review E*, 59:R4737–R4740, 1999.

[16] J.P. Gao, W.D. Luedtke, and U. Landman. Structures, solvation forces and shear of molecular films in a rough nano-confinement. *Tribology Letters*, 9:3–13, 2000.

[17] O. M. Braun and Y. S. Kivshar. *The Frenkel-Kontorova Model*. Springer, Berlin Heidelberg, 2004.

[18] Y. Braiman, J. Barhen, and V. Protopopescu. Control of friction at the nanoscale. *Physical Review Letters*, 90(9):094301.1–094301.4, 2003.

[19] H. Hlscher, U. D. Schwarz, and R. Wiesendanger. Simulation of a scanned tip on a naf(001) surface in friction force microscopy. *Europhysics Letters*, 36(1):19–24, 1996.

[20] T. Baumberger and C. Caroli. A phenomenology of boundary lubrication: the lumped junction model. *European Physical Journal B*, 4:13–23, 1998.

[21] S. P. Bhat and D. S. Bernstein. Continuous finite-time stabilization of the translational and rotatinal double integrators. *IEEE Trans. Automat. Contr.*, 43(5):678–682, 1998.

[22] S. P. Bhat and D. S. Bernstein. Finite-time stability of continuous autonomous systems.

SIAM J. Control Optim., 38(3):751–766, 2000.

[23] Y. Guo, Z. Qu, and Z. Zhang. Lyapunov stability and precise control of the frictional dynamics of a one-dimensional nanoarray. *Physical Review B*, 73(9):094118.1–094118.5, 2006.

[24] H. Khalil. *Nonlinear Systems*. Prentice Hall, 3rd edition, 2002.

[25] Z. Qu. *Robust Control of Nonlinear Uncertain Systems*. Wiley Sciences in Nonlinear Science. John Wiley & Sons, 1998.

[26] Y. Guo and Zhihua Qu. Control of frictional dynamics of a one-dimensional particle array. *Automatica*, to appear.

[27] J. J. E. Slotine and W. Li. *Applied Nonlinear Control*. Prentics Hall, New Jersey, 1991.

[28] C. Godsil and G. Royle. *Algebraic Graph Theory*. Springer, New York, 2001.

[29] C. W. Wu. *Synchronization in Coupled Chaotic Circuits and Systems*. World Scientific, Singapore, 2002.

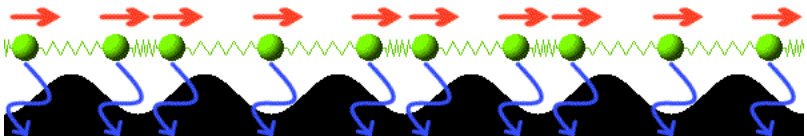

Figure 1. The Frenkel-Kontorova model. The model describes a harmonic chain (mimic a layer of nano-particles) in a spatially periodic potential (mimic the substrate). The chain is driven by a constant force and the dynamics is damped by a velocity-proportional damping.

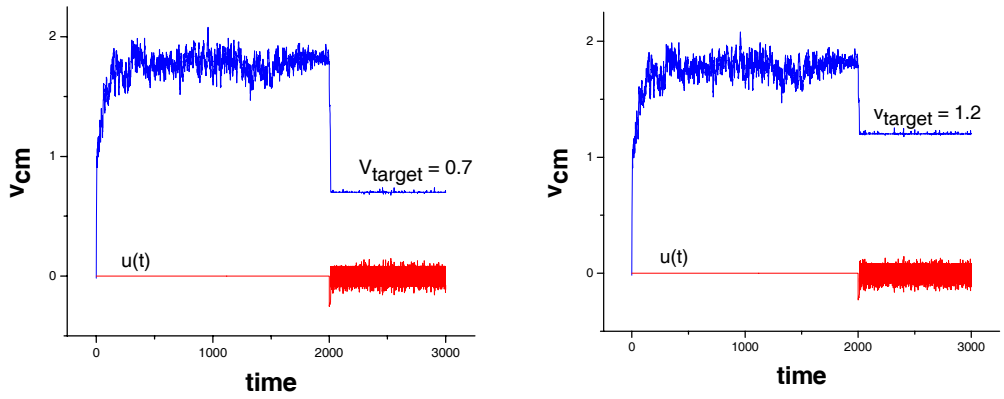

(a) (b)

Figure 2. Performance of the non-Lipschitzian control (13) for a 128-particle system. Control is initiated at $t = 2000$. The blue lines show the time series of the center of mass velocities and the red lines show the control input. The parameters are $\gamma = 0.1, \kappa = 0.26, f = 0.3, \alpha = 0.25, \xi = 1/7$.

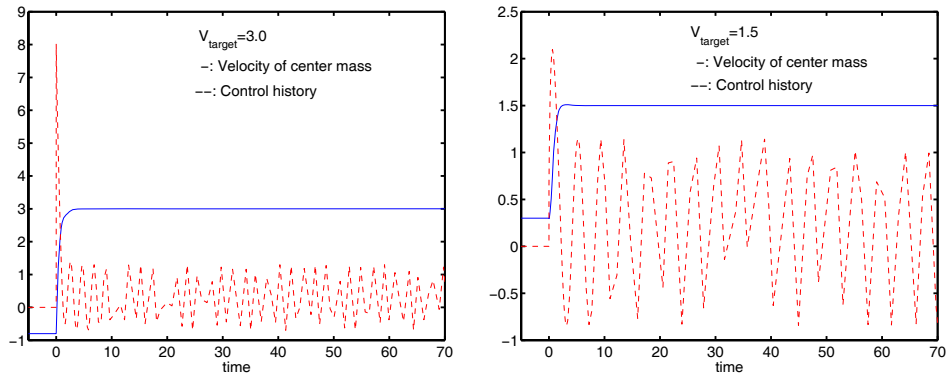

(a) (b)

Figure 3. Performance of the Lyapunov-based control (17) for a 15-particle system. Control is initiated at $t = 0$. The commanded values are 3.0 for (a) and 1.5 for (b). The parameters are $\gamma = 0.1, \kappa = 0.26, f = 0, k_1 = 5.07, k_2 = 4.7$.

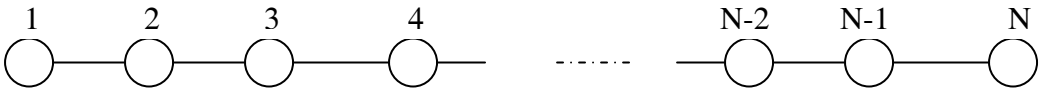

Figure 4. Connectivity of the particles. The bidirectional graph shows a nearest-neighbor structure, whose Laplacian matrix is strongly connected. The property is used in establishing local stability of the open-loop system.

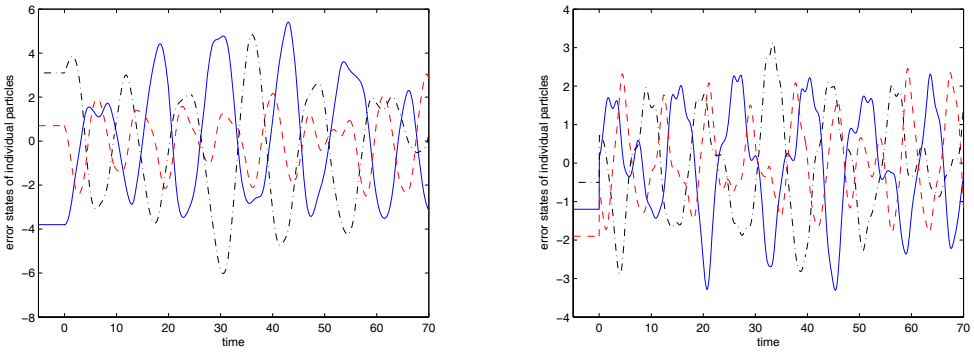

(a) (b)

Figure 5. Particles dynamics of the average system tracking the commanded average velocity $v_{target} = 1.5$. (a) The phase variables of individual particles, (b) the velocity variables of individual particles. Dynamics of single particles is unstable though the average system is stable.

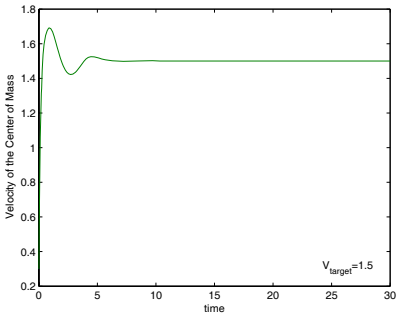

(a)

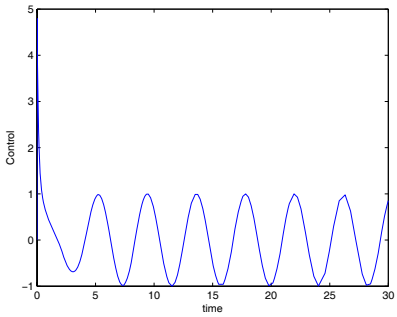

(b)

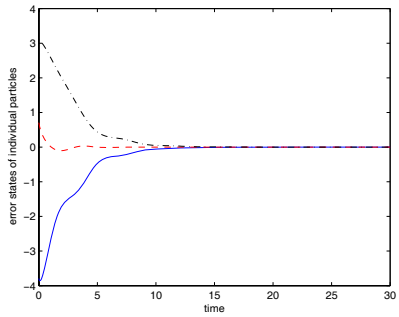

(c)

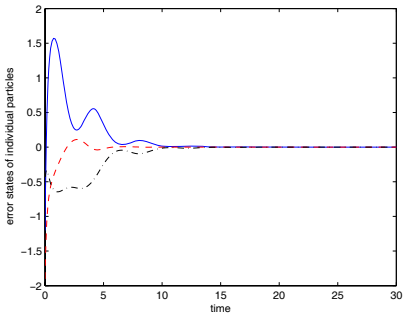

(d)

Figure 6. Tracking performance of single particles in a three-particle system. The commanded value is $v_{target} = 1.5$. The system parameters are $\gamma = 4, \kappa = 1.5$, and the control parameters are $k_1 = 5.8, k_2 = 4$. (a) The time history of the velocity of the center of the mass, (b) the control history, (c) the error variables between commanded positions and particle positions, (d) the error variables between commanded velocities and particle velocities.

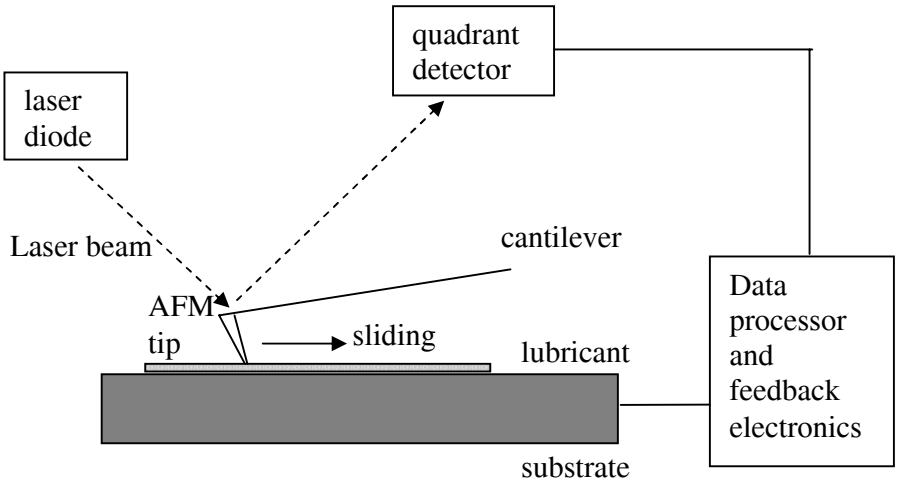

Figure 7. A schematic illustration of AFM experimental setup for feedback control of friction. A very small tip attached on a cantilever is drawn across a surface. The surface is systematically scanned line by line. The tip is bent by the forces between the tip and the surface. This motion of the tip is detected with the laser beam deflection method. The position of the beam is detected with a four quadrant photodetector.

AUTHOR'S BIO

Yi Guo received her Ph.D. degree from the University of Sydney, Australia, in 1999. She is an Assistant Professor in the Department of Electrical and Computer Engineering at Stevens Institute of Technology. Prior to joining Stevens in 2005, she was a visiting Assistant Professor in the Department of Electrical and Computer Engineering at University of Central Florida. From 2000 to 2002, she was a Research Fellow in the Computer Science and Mathematics Division of Oak Ridge National Laboratory. Her main research interests are in nonlinear control, mobile robotic systems, cooperative and decentralized control, and control applications. Dr. Guo is a Senior Member of IEEE. Her mailing address is Department of Electrical and Computer Engineering, Stevens Institute of Technology, Hoboken, NJ 07030. Her email is *yguo1@stevens.edu*.

Zhihua Qu received his Ph.D. degree in electrical engineering from the Georgia Institute of Technology in 1990. Since then, he has been with the University of Central Florida. Currently, he is a Professor in the School of Electrical Engineering and Computer Science. His main research interests are nonlinear systems and control, cooperative control, robust and adaptive control designs, and robotics. He has published a number of papers in these areas and is the author of two books, *Robust Control of Nonlinear Uncertain Systems* by Wiley Interscience and *Robust Tracking Control of Robotic Manipulators* by IEEE Press. He is presently serving as an Associate Editor for *Automatica* and for *International Journal of Robotics and Automation*.

Yehuda Braiman received his Ph.D. from the Tel Aviv University in 1993. He is a Senior Research Staff at the Center for Engineering Science Advanced Research, Computer Science and

Mathematics Division at the Oak Ridge National Laboratory. Prior to joining ORNL, he was a visiting Assistant Professor at Emory University and a Postdoctoral Fellow at Georgia Institute of Technology and at Emory University. Dr. Braiman's main interests include modeling fracture propagation in metallic glasses, friction and control of friction at the atomic scale, coherent beam combining of arrays of high power semiconductor lasers, and nonlinear dynamical systems. He is a member of the APS and MRS.

Zhenyu Zhang received his Ph.D. degree in condensed matter theory from Rutgers University in 1989. He is now a Distinguished Research Scientist in the Materials Science and Technology Division of Oak Ridge National Laboratory and Professor of Physics at the University of Tennessee (Joint Faculty). His research focuses on theoretical understanding of the formation, stability, properties, and potential applications of low-dimensional materials. He is a Fellow of the American Physical Society and currently serves on the editorial boards of *Physical Review Letters, Chinese Physics Letters*, and *ACTA PHYSICA SINICA*.

Jacob Barhen is a UT-Battelle Corporate Fellow and, since 1994, director of the Center for Engineering Science Advanced Research at the Oak Ridge National Laboratory. He is also a nonresident affiliate of Caltech's Jet Propulsion Laboratory and an adjunct professor in the Department of Computer Science at the University of Tennessee, Knoxville. From 1987 to 1994, he was the head of the Neural Computation and Nonlinear Science Group at Caltech/JPL. He began his career at ORNL, where he headed the Machine Intelligence Group from 1978 to 1987. Currently, the Missile Defense Agency, the Office of Naval Research, the DOE Office of Science, the Naval Sea Systems Command, and other US Government agencies support his work. His present research interests include emerging computational systems, global optimization,

sensitivity and uncertainty analysis, neural networks, and signal processing. He has authored more than 170 scientific papers and holds eight US patents. He has received three NASA Space Act awards for major contributions to the National Space Program, 11 NASA awards for Technical Innovation, and a 1998 R&D-100 award, for the invention of the TRUST global optimization method. He is a member of the editorial boards of the *International Journal of Distributed Sensor Networks, Neural Processing Letters, Neural Networks, Mathematical and Computer Modeling*, and *Concurrency and Computation*. He is a member of the AAAS, IEEE, SPIE, the International Neural Networks Society, and the Planetary Society. He received his Doctorate from the Technion - Israel Institute of Technology in 1978.